Efficient Aeroelastic Reduced Order Model with Global Modifications of the Structure

Gang Chen [a,1], Dongfeng Li [a,b], Qiang Zhou [a,c], Andrea Da Ronch [d], Yueming Li [a,b]

a. State Key Laboratory for Strength and Vibration of Mechanical Structures, School of Aerospace, Xi'an Jiaotong University, Xi'an, 710049, China
b. Shaanxi Key Laboratory for Environment and Control of Flight Vehicle, School of Aerospace, Xi'an Jiaotong University, Xi'an, 710049, China
c. No. 38 Research Institute of China Electronics Technology Group Corporation, Hefei, 230088, China
d. Engineering and the Environment, University of Southampton, Southampton SO17 1BJ, UK

ABSTRACT

Time domain aeroelastic analysis has high computing costs when using computational fluid dynamics. These costs become prohibitive when the structural model undergoes large changes from the baseline design, as within an aircraft design process. To overcome this realistic challenge, we have developed, implemented, and demonstrated an efficient method that is robust in the presence of global modifications of the structure. The method consists of: a) a reduced order model of the linearized Navier-Stokes equations generated around an aeroelastic equilibrium that depends, in turn, on the structural model; b) an approximate structural dynamic reanalysis method valid for global modifications of the structure; and c) a mechanism to exchange information between fluid and structural solvers without need for calculating at each iteration of the structural design an eigenvalue problem of the modified structure. The resulting aeroelastic reduced order model is demonstrated for the AGARD 445.6 wing, and material properties are varied up to 100% from their original values. It is found that: a) predictions of the time domain aeroelastic response and of the flutter speed are accurate for all modifications of the structure; and b) the computational efficiency of the proposed aeroelastic reduced order model is linearly proportional to the number of structural configurations considered. The method, therefore, is ideally suited for optimization and uncertainty studies.

Keywords: reduced order model, proper orthogonal decomposition, computational fluid dynamics, global structural modification, flutter boundary, time domain analysis.

1. Introduction

Aeroelastic analysis in the transonic regime is a critical aspect of today's aircraft design process. In transonic flow, linear aerodynamic theories fail due to the presence of flow nonlinearities (e.g. shocks, separation). Computational fluid dynamics (CFD) has become a feasible alternative [1, 2] to linear methods for the capability to model flow nonlinearities. This comes at the price of high computing times, and CFD-based aeroelastic analysis is generally restricted to few flight conditions and mass configurations [3, 4].

[1] Professor. Corresponding author. Email: aachengang@xjtu.edu.cn

To overcome the costs involved in solving complex fluid models of large size, researchers have developed CFD-based unsteady aerodynamic reduced order models (ROMs). These models extract key data of the fluid systems to generate a low dimensional system that retains similar accuracy of the full order model while reducing significantly the costs. System identification [5-7] and proper orthogonal decomposition (POD) are among the most popular ROMs for nonlinear aeroelastic analysis. For example, Dowell [8] and Lucia [9] demonstrated the use of ROMs to investigate transonic limit-cycle oscillation (LCO). Reference [10] documented a ROM for gust analysis in the transonic regime, providing a fast identification of the worst-case gust. The POD method, in particular, has been successfully applied to the aeroelastic analysis of turbine blades [11, 12]， helicopter rotor blade [13], wings [14-16] and complete aircraft configurations [17, 18]. More recently, the POD has been exercised for transonic aeroelastic analysis [19], active aeroelastic control [20], LCO control [21], gust response analysis [22], and transonic flutter suppression with control delay [23].

The largest efforts in the ROM community are addressed at improving the model predictions at a fixed flight condition for a frozen aeroelastic model configuration. Changes to either flight conditions (e.g. Mach number, angle of attack) or model configuration (e.g. mass, geometry) are neglected for the difficulty of accounting for these effects within a single ROM. The limited body of work on this topic consists of the following publications available in the open literature. Epureanu [24] and Lieu [25-27] used ROMs to predict the transonic aeroelastic response with variations of the free stream Mach number and angle of attack. Chen [28] proposed a nonlinear POD technique, Chen [29] discussed a support-vector-machine based ROM, and Chen [30] presented a linear parameter-varying (LPV) method valid for bounded changes of the flow conditions. Winter [31] presented a novel aerodynamic ROM approach for predicting generalized aerodynamic forces (GAF) based on local linear neuro-fuzzy models considering variations of Mach number. Even fewer studies have shown the ability to capture changes in the mass and stiffness distribution of an aircraft structure within a single aeroelastic ROM. As the aircraft design process proceeds, with the outer shape being frozen at the early stages, the structural model undergoes multiple changes to guarantee the design target loads are met. Structural modeshapes and associated frequencies are dependent upon the mass and stiffness distribution, and this should be correctly included in an aeroelastic analysis, Hayes [32]. When a structural modification is made, the structural model need to be updated and the new modeshapes and frequencies recalculated. In an aeroelastic analysis, the influence of changes in the structural model will also propagate to the fluid

solution, with both mean and unsteady flow components depending upon the structural model. One approach to update the aeroelastic ROM, referred to as the direct method herewith, is the regeneration of the model. For every change of the structural model, this entails calculating: a) the new set of modeshapes and frequencies; b) the mean flow solution that guarantees the aeroelastic equilibrium for the modified structure; and c) the ROM around the new equilibrium position. To overcome the related computational expense, Fenwick [33] used a linear interpolation on a set of available ROMs to obtain a new ROM without regeneration. This approach was shown for the flutter boundary prediction with changes to the local mass distribution (e.g. fuel load distribution). Voss [34] used several synthetic modeshapes that were chosen to exhibit all realistic structural modes. Various unsteady CFD computations were run to generate the ROM database, including dependencies on Mach number, reduced frequency and modeshapes. Zhang [35] demonstrated a method to obtain a new ROM using an existing CFD-based auto regressive with eXogenous input (ARX) model based on radial basis function (RBF) interpolation for local changes of the root boundary condition. Winter [36] presented two novel CFD-based ROMs robust to variations in the structural modeshapes due to additional lumped mass.

Most of the studies in the previous paragraphs neglected the case where structural modifications are made at global level, and instead focused the attention to local structural modifications. Global changes to the structural parameters are routinely done in the aircraft design process following optimization and trade-off studies. As the first step, the global level analysis initializes all the global quantities and responses, and then provides information to the local level sub-problem. At the global level, wing modifications consist generally of changes to the mass and stiffness distribution to meet the design target loads [37, 38]. This specific problem calls for an efficient ROM formulation that can investigate the impact that structural modifications have on the aeroelastic analysis, uncertainty quantification, and optimization design.

The novelty of the work detailed in this paper is the development and implementation of a time domain aeroelastic ROM valid for global modifications of the structure. The methodology avoids the computational burden traditionally associated with direct methods that solve a normal mode analysis at each modification of the structure. On the contrary, the proposed methodology leverages on a structural dynamics reanalysis that provides a rapid approximation of the dynamics of the modified structure, and this feature is embedded within a CFD-based aeroelastic ROM, referred to as the approximate method.

The paper continues in Section 2 with a description of the aeroelastic ROM generation. Section 3

provides a background knowledge on the structural dynamics reanalysis for global modifications of the structure, and discusses the introduction of this feature within the CFD-based aeroelastic ROM. Section 4 presents the impact that global structural modifications of the AGARD 445.6 wing have on the time domain aeroelastic response and flutter boundary. Furthermore, this Section quantifies the advantages, measured in terms of accuracy and computational cost, of the proposed approach compared to the existing one. Finally, conclusions are given in Section 5.

2. Reduced Order Model of Large Scale Aeroelastic System

2.1 Flow and Structural Solvers

The nonlinear aeroelastic system is formulated using the two-field arbitrary Lagrangian-Eulerian (ALE) approach. The governing equations are

$$\frac{d(\mathbf{A}\cdot\mathbf{w})}{dt}+\mathbf{F}(\mathbf{w})=\mathbf{0} \tag{1}$$

$$\mathbf{M}\ddot{\mathbf{d}}+\mathbf{D}\dot{\mathbf{d}}+\mathbf{K}\mathbf{d}=\mathbf{f} \tag{2}$$

where Eq. (1) represents a finite volume discretization of the ALE non-dimensional conservative form of the Navier–Stokes equations. Here, **A** is a diagonal matrix containing the cell volumes, **F** is the nonlinear numerical flux function, **w** is the vector of conservative flow variables, and **d** is the vector of structural displacements. Eq. (2) is for a finite element discretization of the structural dynamic equations. **M**, **D**, and **K** are the mass, damping, and stiffness matrices, respectively. **f** is the vector of aerodynamic loads calculated at the structural grid points, derived from solving Eq. (1).

The CFD solver employs Cartesian grids, using a multi-block structured cell-centered finite volume discretisation, and the second-order Van Leer scheme [39] is used for the spatial discretization. The dual time-stepping [40] and Lower-Upper Symmetric Gauss-Seidel (LU-SGS) implicit method [41] are used for time integration.

A modal representation of the structural model is assumed, without restricting the validity of the approach presented herein. Using generalized (or modal) coordinates, **u**, the structural displacement field is expressed in the canonical form, $\mathbf{d}=\mathbf{\Phi u}$, where $\mathbf{\Phi}=[\boldsymbol{\phi}^1,\ \boldsymbol{\phi}^2,\ ...]$ denotes the modal matrix. Using generalized coordinates, Eq. (2) becomes:

$$\bar{\mathbf{M}}\cdot\ddot{\mathbf{u}}+\bar{\mathbf{D}}\cdot\dot{\mathbf{u}}+\bar{\mathbf{K}}\cdot\mathbf{u}=\mathbf{f}_{gen} \tag{3}$$

where $\bar{\mathbf{M}}=\mathbf{\Phi}^T\mathbf{M}\mathbf{\Phi}$, $\bar{\mathbf{D}}=\mathbf{\Phi}^T\mathbf{D}\mathbf{\Phi}$ and $\bar{\mathbf{K}}=\mathbf{\Phi}^T\mathbf{K}\mathbf{\Phi}$ are the generalized mass, damping and stiffness matrices, respectively. $\mathbf{f}_{gen}$ is the vector of generalized aerodynamic forces:

$$\mathbf{f}_{gen} = \mathbf{\Phi}^T \mathbf{f} \text{ or for the vector element } i\text{: } \mathbf{f}_{gen}^i = q_\infty \cdot \int_{\mathbf{s}} c_p \cdot \boldsymbol{\phi}^i \circ d\mathbf{S} \tag{4}$$

where $\mathbf{f}_{gen}^i$ is i-th generalized aerodynamic force, q_∞ is the free stream dynamic pressure, and c_p is pressure coefficient.

2.2 Coupling algorithm

A time domain, fully-implicit, loosely-coupled partitioned approach is employed for the unsteady fluid-structure interaction (FSI) analysis. The process is depicted in **Fig. 1**. A converged steady-state flow solution is used to initialize the FSI loop. The transfer of the aerodynamic loads from the fluid to the structural field, and the transfer of the structural displacements from the structural to the aerodynamic field are performed using the infinite plate spline (IPS) method [42]. The radial basis functions (RBFs), combined with the transfinite interpolation (TFI) algorithm [43], are then used to warp the fluid volume mesh, based on the new deformed surface grid obtained by mapping the structural displacements onto the fluid surface grid. The iterative process continues until the change in the structural displacements between two consecutive iterations is below a given threshold, or the maximum number of iterations is reached. The coupled aeroelastic solver has been exercised on several two and three-dimensional aeroelastic models. The reader is referred to [19, 23, 44] for more details.

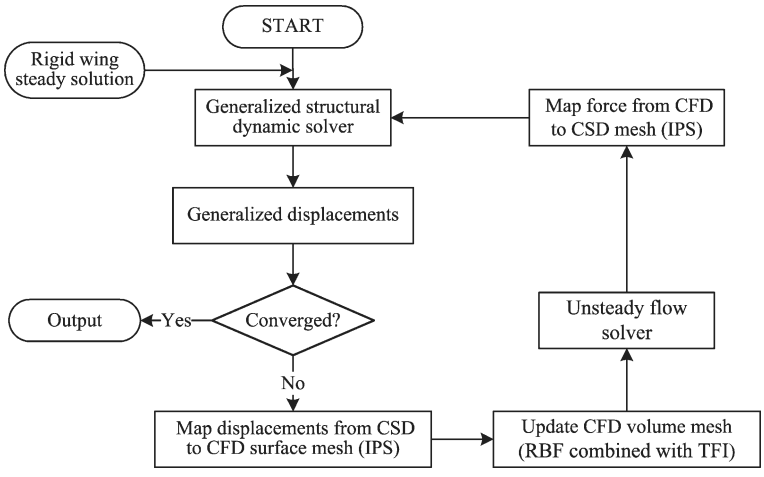

Fig. 1 Schematic of the fluid-structure coupling algorithm; 'CSD' indicates computational structural dynamics.

2.3 Unsteady Aerodynamics Reduced Order Model

The POD method is the method of choice to provide a compact description of large scale computational models as in the case of unsteady transonic flows for aeroelastic analysis [45, 46]. To start with, the unsteady flow equations are linearized around a mean solution (equilibrium). The linearized flow solver is then used to obtain the POD snapshots for the generation of the unsteady aerodynamics

ROM. Denoting $\Delta\mathbf{w}, \Delta\mathbf{u}, \Delta\dot{\mathbf{u}}$ small perturbation around the equilibrium $\mathbf{w}_0, \mathbf{u}_0, \dot{\mathbf{u}}_0$, one obtains the linearized flow equations:

$$\mathbf{A}_0\dot{\mathbf{w}} + \mathbf{H}\mathbf{w} + (\mathbf{E}+\mathbf{C})\dot{\mathbf{u}} + \mathbf{G}\mathbf{u} = \mathbf{0} \tag{5}$$

where

$$\mathbf{H} = \frac{\partial \mathbf{F}}{\partial \mathbf{w}}(\mathbf{w}_0, \mathbf{u}_0, \dot{\mathbf{u}}_0) \qquad \mathbf{G} = \frac{\partial \mathbf{F}}{\partial \mathbf{u}}(\mathbf{w}_0, \mathbf{u}_0, \dot{\mathbf{u}}_0)$$

$$\mathbf{E} = \frac{\partial \mathbf{A}}{\partial \mathbf{u}}\mathbf{w}_0 \qquad \mathbf{C} = \frac{\partial \mathbf{F}}{\partial \dot{\mathbf{u}}}(\mathbf{w}_0, \mathbf{u}_0, \dot{\mathbf{u}}_0)$$

The matrix **H** is the gradient of the numerical flux function with respect to the vector of fluid variables. Matrices **G** and **C** are the gradients of the flux function with respect to the generalized coordinates and their velocities, respectively. Finally, the matrix **E** indicates the gradient of the cell volumes with respect to the generalized coordinates. Note that the matrices **G**, **E** and **C** need to be re-computed if the structural parameters are modified.

The linearization of the structural dynamic equations around the equilibrium point is:

$$\bar{\mathbf{M}}\ddot{\mathbf{u}} + \bar{\mathbf{D}}_0\dot{\mathbf{u}} + \bar{\mathbf{K}}_s\mathbf{u} = \mathbf{P}_0\mathbf{w} \tag{6}$$

where

$$\bar{\mathbf{K}}_0 = \frac{\partial \mathbf{f}^{int}}{\partial \mathbf{u}}(\mathbf{u}_0, \dot{\mathbf{u}}_0) \qquad \bar{\mathbf{K}}_s = \bar{\mathbf{K}}_0 - \frac{\partial \mathbf{f}^{ext}}{\partial \mathbf{u}}(\mathbf{w}_0, \mathbf{u}_0)$$

$$\bar{\mathbf{D}}_0 = \frac{\partial \mathbf{f}^{int}}{\partial \dot{\mathbf{u}}}(\mathbf{u}_0, \dot{\mathbf{u}}_0) \qquad \mathbf{P}_0 = \frac{\partial \mathbf{f}^{ext}}{\partial \mathbf{w}}(\mathbf{w}_0, \mathbf{u}_0)$$

The terms $\frac{\partial \mathbf{f}^{ext}}{\partial \mathbf{u}}$ and $\bar{\mathbf{D}}_0$ are neglected to analyze the system stability, which is studied as an eigenvalue problem:

$$\bar{\mathbf{M}}\ddot{\mathbf{u}} + \bar{\mathbf{K}}_0\mathbf{u} = \mathbf{P}_0\mathbf{w} \tag{7}$$

Using the linearized flow and structural equations derived in Eqs. (5) and (7), the generalized eigenvalue problem is:

$$(\mathbf{N} - \zeta_i\boldsymbol{\Theta})\mathbf{q}_i = \mathbf{0} \tag{8}$$

where ζ_i indicates the *i*-th eigenvalue and $\mathbf{q}_i$ the corresponding eigenvector, and

$$\mathbf{N} = \begin{bmatrix} \mathbf{H} & (\mathbf{E}+\mathbf{C}) & \mathbf{G} \\ -\mathbf{P} & \mathbf{0} & \mathbf{K}_0 \\ \mathbf{0} & \mathbf{I} & \mathbf{0} \end{bmatrix}, \quad \boldsymbol{\Theta} = \begin{bmatrix} \mathbf{A} & \mathbf{0} & \mathbf{0} \\ \mathbf{0} & \mathbf{M} & \mathbf{0} \\ \mathbf{0} & \mathbf{0} & \mathbf{I} \end{bmatrix}, \quad \mathbf{q} = \begin{bmatrix} \mathbf{w} \\ \dot{\mathbf{u}} \\ \mathbf{u} \end{bmatrix}.$$

It is worth noting here that the unsteady flow equations are described by a ROM obtained from a

POD of the linearized fluid equations. The POD method aims at reconstructing the behavior of the overall system using an orthogonal basis set with a much smaller number of degrees of freedom. Denote $\{\mathbf{x}^k\}$, for $k = 1,2,3\ldots m$, a set of *m* snapshots, where $\mathbf{x}^k$ belongs to an *n*-dimensional space. The POD method searches an *m*-dimensional proper orthogonal subspace, $\mathbf{\Psi} \in \mathbf{R}^{n\times m}$, where $m < n$, to minimize the mapping errors from $\mathbf{\Psi}$

$$\mathbf{G} = \min_{\mathbf{\Phi}} \sum_{k=1}^{m} \left\| \mathbf{x}^k - \mathbf{\Omega}\mathbf{\Omega}^T \mathbf{x}^k \right\| = \sum_{k=1}^{m} \left\| \mathbf{x}^k - \mathbf{\Psi}\mathbf{\Psi}^T \mathbf{x}^k \right\| \tag{9}$$

where $\mathbf{\Omega}$ is an arbitrarily chosen subspace, which satisfies $\mathbf{\Omega}^H\mathbf{\Omega} = \mathbf{I}$. The minimization problem is equivalent to

$$\mathbf{H} = \max_{\mathbf{\Phi}} \sum_{k=1}^{m} \frac{\left\langle \left(\mathbf{x}^k, \mathbf{\Omega}\right)^2 \right\rangle}{\left\|\mathbf{\Omega}\right\|^2} = \sum_{k=1}^{m} \frac{\left\langle \left(\mathbf{x}^k, \mathbf{\Psi}\right)^2 \right\rangle}{\left\|\mathbf{\Psi}\right\|^2}, \quad \mathbf{\Omega}^H\mathbf{\Omega} = \mathbf{I} \tag{10}$$

where the $\langle\cdot\rangle$ indicates an averaging operation, and $(\cdot,\cdot)$ indicates an inner product operation. The constraint optimization problem in Eq. (10) is transformed into the following Lagrange equation

$$J\left(\mathbf{\Omega}\right) = \sum_{k=1}^{m} \left(\mathbf{x}^k, \mathbf{\Omega}\right)^2 - \lambda\left(\left\|\mathbf{\Omega}\right\|^2 - 1\right) \tag{11}$$

Solving the partial derivative of the objective function $J(\mathbf{\Omega})$ with respect to $\mathbf{\Omega}$ gives

$$\frac{d}{d\mathbf{\Omega}} J\left(\mathbf{\Omega}\right) = 2\mathbf{X}\mathbf{X}^H\mathbf{\Omega} - 2\lambda\mathbf{\Omega} \tag{12}$$

where $\mathbf{X} = \{\mathbf{x}_1, \mathbf{x}_2, \cdots \mathbf{x}_m\} \in \mathbf{R}^{n\times m}$ is a matrix with columns equal to the *m* snapshots. One finds that the solution to Eq. (12) is:

$$\left(\mathbf{X}\mathbf{X}^T - \xi\mathbf{I}\right)\mathbf{\Psi} = 0 \tag{13}$$

The above equation involves the solution of a large-scale eigenvalue problem of the POD kernel, $\mathbf{X}\mathbf{X}^H \in \mathbf{R}^{n\times n}$. Because $\mathbf{X}\mathbf{X}^H$ and $\mathbf{X}^H\mathbf{X}$ have the same eigenvalues, $\mathbf{\Psi}$ is obtained from the following equation:

$$\begin{cases} \mathbf{X}\mathbf{X}^T\mathbf{V} = \mathbf{V}\mathbf{\Lambda} \\ \mathbf{\Psi} = \mathbf{X}\mathbf{V}\mathbf{\Lambda}^{-1/2} \end{cases} \tag{14}$$

where $\mathbf{\Psi} = [\boldsymbol{\psi}_1, \boldsymbol{\psi}_2, \ldots, \boldsymbol{\psi}_m]$, $\mathbf{\Lambda} = diag(\xi_1, \xi_2 \cdots \xi_m)$, $\xi_1 \geq \xi_2 \geq, \ldots, \geq \xi_m$. The value of ξ_i represents the contribution of the *i*-th snapshot to the original system. In practice, the generation of an aeroelastic ROM includes the first *r* POD modes, $\mathbf{\Psi}_r = [\boldsymbol{\psi}_1, \boldsymbol{\psi}_2, \ldots, \boldsymbol{\psi}_r]$, that retain most of the energy of the original system. By projecting the full-order series $\mathbf{x}^{n\times 1}$ onto the *r* POD modes, a model of size *r* is obtained

$$\begin{cases} \dot{\mathbf{x}}_r = \boldsymbol{\Psi}_r^T \mathbf{A} \boldsymbol{\Psi}_r \mathbf{x}_r + \boldsymbol{\Psi}_r^T \mathbf{B} \mathbf{y} \\ \mathbf{f}^{ext} = \mathbf{C} \boldsymbol{\Psi}_r \mathbf{x}_r \end{cases} \tag{15}$$

where $\mathbf{A} = -\mathbf{A}_0^{-1}\mathbf{H}$, $\mathbf{B} = -\mathbf{A}_0^{-1}\left[\mathbf{E} + \mathbf{C}\ \ \mathbf{G}\right]$, $\mathbf{y} = \left[\dot{\mathbf{u}}\ \ \mathbf{u}\right]^T$, $\mathbf{C} = \mathbf{P}$. Here, **A**, **B**, and **y** can be considered as the system inputs, and the $\mathbf{f}^{ext}$ is the system output.

The above steps outline the process of generating an unsteady aerodynamics ROM for given modeshapes. The resulting aeroelastic model is obtained by coupling the structural dynamic equations, Eq. (7), with Eq. (15) for the ROM of the fluid.

3. Aeroelastic Reduced Order Model in the Presence of Global Structural Modifications

3.1 Approximate structural dynamic reanalysis method

In any optimization activity involving changes to the structural model, the modal characteristics of the structure (frequencies, damping, and modeshapes) change. Generally, modal characteristics are obtained from a normal mode analysis (eigenvalue problem), which may become computationally expensive for a large-scale system if repeated for many optimization evaluations. To overcome this challenge, several methods, commonly classified into two categories, were proposed to ease the eigenvalue reanalysis for the modified structure [47]. The first category includes direct methods, commonly based on the Sherman-Morrison-Woodbury (SMW) formula [48], that are applicable for large but local (or low-rank) modifications. The drawback of these methods is that they are limited by the scale of the problem or rank of the modification, and are not adequate for global modifications of the structural parameters. Direct methods also suffer from high computational costs. On the contrary, the second category collects approximate methods [49-51] that aim at obtaining the frequencies and modeshapes for the modified structures without resolving an eigenproblem each time. The advantage in doing so is a significant reduction of the computational costs as well as an extended applicability of the methods for global (or high-rank) modifications of the structures. The extended Kirsch combined method [50, 52] is an efficient approach for the case of large modifications of the structural parameters. More details relevant to this work are given in the remainder of this section.

Consider initially a structure with a nominal stiffness matrix, $\mathbf{K}_0$, and mass matrix, $\mathbf{M}_0$. Frequencies, λ_0^i, and modeshapes, $\boldsymbol{\Phi}_0 = [\boldsymbol{\phi}_0^1, \boldsymbol{\phi}_0^2, ...]$, are calculated by solving the generalized eigenproblem:

$$\mathbf{K}_0 \boldsymbol{\phi}_0^i = \lambda_0^i \mathbf{M}_0 \boldsymbol{\phi}_0^i \tag{16}$$

that is referred to as the original problem (indicated by the subscript 0). When the structural parameters are modified, the stiffness and mass matrices are perturbed into the form $\mathbf{K}_0 + \Delta\mathbf{K}$ and $\mathbf{M}_0 + \Delta\mathbf{M}$, respectively. The terms $\Delta\mathbf{K}$ and $\Delta\mathbf{M}$ are the perturbations to the original stiffness and mass matrices. For the modified structure, the eigenvalue problem becomes:

$$\mathbf{K}\boldsymbol{\phi}^i = \lambda^i \mathbf{M}\boldsymbol{\phi}^i \tag{17}$$

where λ^i is the *i*-th eigenvalue of the modified structure, and $\boldsymbol{\phi}^i$ is the *i*-th eigenvector of the modified structure.

The extended Kirsch combined method uses the second-order eigenvector terms [53] as the basis vectors in the following modeshapes reduced basis:

$$\boldsymbol{\phi}^i = \boldsymbol{\phi}_B^i \mathbf{z}^i \tag{18}$$

where

$$\boldsymbol{\phi}_B^i = \left[\boldsymbol{\phi}_0^i,\ \boldsymbol{\phi}_1^i,\ \boldsymbol{\phi}_2^i\right] \tag{19}$$

$$\mathbf{z}^i = (z_0^i,\ z_1^i,\ z_2^i)^T \in \mathbf{R}^{3\times 1} \tag{20}$$

$$\boldsymbol{\phi}_1^i = \sum_{s=1,s\neq i}^{n} \frac{1}{\lambda_0^i - \lambda_0^s}[(\boldsymbol{\phi}_0^s)^T(\Delta\mathbf{K} - \lambda_0^i\Delta\mathbf{M})\boldsymbol{\phi}_0^i]\boldsymbol{\phi}_0^s - \frac{1}{2}[(\boldsymbol{\phi}_0^i)^T\Delta\mathbf{M}\boldsymbol{\phi}_0^i]\boldsymbol{\phi}_0^i = \boldsymbol{\phi}_0\mathbf{Z}_1^i \tag{21}$$

$$\begin{aligned}\boldsymbol{\phi}_2^i = &\sum_{s=1,s\neq i}^{n} \frac{1}{\lambda_0^i - \lambda_0^s}[(\boldsymbol{\phi}_0^s)^T(\Delta\mathbf{K} - \lambda_0^i\Delta\mathbf{M})\boldsymbol{\phi}_1^i - \lambda_1^i(\boldsymbol{\phi}_0^s)^T(\mathbf{M}_0\boldsymbol{\phi}_1^i + \Delta\mathbf{M}\boldsymbol{\phi}_0^i)]\boldsymbol{\phi}_0^s \\ &-\frac{1}{2}[(\boldsymbol{\phi}_0^i)^T\Delta\mathbf{M}\boldsymbol{\phi}_1^i + (\boldsymbol{\phi}_1^i)^T(\mathbf{M}_0\boldsymbol{\phi}_1^i + \Delta\mathbf{M}\boldsymbol{\phi}_0^i)]\boldsymbol{\phi}_0^i = \boldsymbol{\phi}_0\mathbf{Z}_2^i\end{aligned} \tag{22}$$

The terms $\boldsymbol{\phi}_1^i$ and $\boldsymbol{\phi}_2^i$ are the *i*-th first and second-order eigenvectors of the modified structure, respectively. The coefficient vector, $\mathbf{z}^i$, consists of three (unknown) elements for a second order perturbation. Substituting Eq. (21) and Eq. (22) into Eq. (18), $\boldsymbol{\Phi}$ can be written as

$$\boldsymbol{\Phi} = \begin{bmatrix} \boldsymbol{\phi}_0^1 \ldots \boldsymbol{\phi}_0^i & \mathbf{0} & \mathbf{0} \\ \mathbf{0} & \boldsymbol{\phi}_0^1 \ldots \boldsymbol{\phi}_0^i & \mathbf{0} \\ \mathbf{0} & \mathbf{0} & \boldsymbol{\phi}_0^1 \ldots \boldsymbol{\phi}_0^i \end{bmatrix} \begin{bmatrix} \mathbf{I}_0^1 \ldots \mathbf{I}_0^i & \mathbf{0} & \mathbf{0} \\ \mathbf{0} & \mathbf{Z}_1^1 \ldots \mathbf{Z}_1^i & \mathbf{0} \\ \mathbf{0} & \mathbf{0} & \mathbf{Z}_2^1 \ldots \mathbf{Z}_2^i \end{bmatrix}^T \begin{bmatrix} \mathbf{z}^1 & \mathbf{0} & \mathbf{0} \\ \mathbf{0} & \mathbf{z}^2 & \mathbf{0} \\ \mathbf{0} & \mathbf{0} & \mathbf{z}^3 \end{bmatrix} = \boldsymbol{\Phi}_0\mathbf{Z} \tag{23}$$

where

$$\mathbf{Z} = \begin{bmatrix} \mathbf{I}_0^1 \ldots \mathbf{I}_0^i & \mathbf{0} & \mathbf{0} \\ \mathbf{0} & \mathbf{Z}_1^1 \ldots \mathbf{Z}_1^i & \mathbf{0} \\ \mathbf{0} & \mathbf{0} & \mathbf{Z}_2^1 \ldots \mathbf{Z}_2^i \end{bmatrix}^T \begin{bmatrix} \mathbf{z}^1 & \mathbf{0} & \mathbf{0} \\ \mathbf{0} & \mathbf{z}^2 & \mathbf{0} \\ \mathbf{0} & \mathbf{0} & \mathbf{z}^3 \end{bmatrix} \tag{24}$$

Substituting Eq. (18) into the eigenvalue problem for the modified structure Eq. (17), and pre-multiplying by $(\boldsymbol{\phi}_B^i)^T$, one obtains:

$$(\boldsymbol{\phi}_B^i)^T(\mathbf{K}_0+\Delta\mathbf{K})\boldsymbol{\phi}_B^i\mathbf{z}^i=\lambda^i(\boldsymbol{\phi}_B^i)^T(\mathbf{M}_0+\Delta\mathbf{M})\boldsymbol{\phi}_B^i\mathbf{z}^i \tag{25}$$

Adopting the short-hand notation

$$\mathbf{K}_R^i=(\boldsymbol{\phi}_B^i)^T(\mathbf{K}_0+\Delta\mathbf{K})\boldsymbol{\phi}_B^i \tag{26}$$

$$\mathbf{M}_R^i=(\boldsymbol{\phi}_B^i)^T(\mathbf{M}_0+\Delta\mathbf{M})\boldsymbol{\phi}_B^i \tag{27}$$

it is apparent that Eq. (25) reduces to a set of three equations

$$\mathbf{K}_R^i\mathbf{z}^i=\lambda^i\mathbf{M}_R^i\mathbf{z}^i \tag{28}$$

Once the coefficient vector $\mathbf{z}^i$ is found, the coefficient matrix $\mathbf{Z}$ is recovered from Eq. (24), and the *i*-th eigenvector of the modified structure is recovered from Eq. (18). Finally, the *i*-th eigenvalue of the modified structure, λ_K^i, is computed using Rayleigh quotient:

$$\lambda_K^i=\frac{(\boldsymbol{\phi}^i)^T(\mathbf{K}_0+\Delta\mathbf{K})\boldsymbol{\phi}^i}{(\boldsymbol{\phi}^i)^T(\mathbf{M}_0+\Delta\mathbf{M})\boldsymbol{\phi}^i} \tag{29}$$

The steps involved in the extended Kirsch combined method are presented in Algorithm 1.

Algorithm 1 Extended Kirsch combined method

1	For the original structure, solve the eigenvalue problem, Eq. (16);
2	For the modified structure, identify the perturbation matrices such that $\mathbf{K}_0+\Delta\mathbf{K}$ and $\mathbf{M}_0+\Delta\mathbf{M}$;
3	Calculate first and second-order perturbations of the eigenvector, using Eqs. (21) and (22);
4	Form the stiffness and mass matrices, $\mathbf{K}_R^i$ and $\mathbf{M}_R^i$, using Eqs. (26) and (27);
5	Solve Eq. (28) for the coefficient vector $\mathbf{z}^i$;
6	Calculate coefficient matrix $\mathbf{Z}$ and *i*-th eigenvector of the modified structure, using Eqs. (18) and (24);
7	Obtain approximated eigenvectors of the modified structure using Eq. (18);

3.2 Aeroelastic ROM for the Modified Structure

In Section 2.3, the unsteady aerodynamics ROM is derived assuming the structural model is frozen, with nominal modeshapes $\boldsymbol{\Phi}_0$. As the matrices of the linearized flow solver, Eq. (5), depend on the generalized coordinates, the unsteady aerodynamics ROM shall be regenerated at each modification of the structure. To this goal, it is convenient to write the physical displacements as

$$\mathbf{d} = \boldsymbol{\Phi}_0(\mathbf{Zu}) \tag{30}$$

where the vector $\mathbf{u}_b = \mathbf{Zu}$ is denoted as the vector of basic generalized displacements. The introduction of this quantity becomes useful in the calculation of the matrices of the linearized flow solver:

$$\mathbf{G} = \frac{\partial \mathbf{F}}{\partial \mathbf{u}}(\mathbf{w}_0, \mathbf{u}_0, \dot{\mathbf{u}}_0) = \frac{\partial \mathbf{F}}{\mathbf{Z}^{-1}\partial \mathbf{u}_b}(\mathbf{w}_0, \mathbf{u}_0, \dot{\mathbf{u}}_0) = \mathbf{ZG}_b$$

$$\mathbf{E} = \frac{\partial \mathbf{A}}{\partial \mathbf{u}}\mathbf{w}_0 = \frac{\partial \mathbf{A}}{\mathbf{Z}^{-1}\partial \mathbf{u}_b}\mathbf{w}_0 = \mathbf{ZE}_b$$

$$\mathbf{C} = \frac{\partial \mathbf{F}}{\partial \dot{\mathbf{u}}}(\mathbf{w}_0, \mathbf{u}_0, \dot{\mathbf{u}}_0) = \frac{\partial \mathbf{F}}{\mathbf{Z}^{-1}\partial \dot{\mathbf{u}}_b}(\mathbf{w}_0, \mathbf{u}_0, \dot{\mathbf{u}}_0) = \mathbf{ZC}_b$$

In state space form, the unsteady aerodynamics ROM in the presence of structural modifications is written as

$$\begin{cases} \dot{\mathbf{x}}_r = \boldsymbol{\Psi}_r^T \mathbf{A} \boldsymbol{\Psi}_r \mathbf{x}_r + \boldsymbol{\Psi}_r^T \mathbf{ZB}_b \mathbf{y} \\ \mathbf{f}^{ext} = \mathbf{ZC}_b \boldsymbol{\Psi}_r \mathbf{x}_r \end{cases} \tag{31}$$

where $\mathbf{A} = -\mathbf{A}_0^{-1}\mathbf{H}$, $\mathbf{B}_b = -\mathbf{A}_0^{-1}\left[\mathbf{E}_b + \mathbf{C}_b \;\; \mathbf{G}_b\right]$, $\mathbf{y} = \left[\dot{\mathbf{u}} \;\; \mathbf{u}\right]^T$, $\mathbf{C}_b = \mathbf{P}_b$. This set of equations is accompanied by the structural dynamic equations of the modified structure:

$$\bar{\mathbf{M}}\ddot{\mathbf{u}} + \bar{\mathbf{K}}\mathbf{u} = \mathbf{f}^{ext} \tag{32}$$

where $\bar{\mathbf{M}} = \mathbf{Z}^T \boldsymbol{\Phi}_0^T (\mathbf{M}_0 + \Delta\mathbf{M}) \boldsymbol{\Phi}_0 \mathbf{Z}$, $\bar{\mathbf{K}} = \mathbf{Z}^T \boldsymbol{\Phi}_0^T (\mathbf{K}_0 + \Delta\mathbf{K}) \boldsymbol{\Phi}_0 \mathbf{Z}$. In the specific case of no structural modifications, $\Delta\mathbf{K} = \mathbf{0}$ and $\Delta\mathbf{M} = \mathbf{0}$, $\mathbf{Z}$ becomes the unity matrix, and Eqs. (32) and (33) are equivalent to Eqs. (15) and (7), respectively. The vector of generalized aerodynamic loads, $\mathbf{f}^{ext}$, is derived from the unsteady aerodynamics ROM. Without the need to re-compute a new POD basis for every structural modification, the calculation of $\mathbf{f}^{ext}$ is inexpensive as it is obtained from a ROM that intrinsically accounts for global modifications of the structural model.

A schematic of the algorithm is illustrated in **Fig. 2**. Within a design environment, the structural parameters are modified iteratively. In this case, the proposed algorithm allows computing rapidly the generalized aerodynamic loads without re-computing, for each structural modification, the POD basis which is used to generate the unsteady aerodynamics ROM.

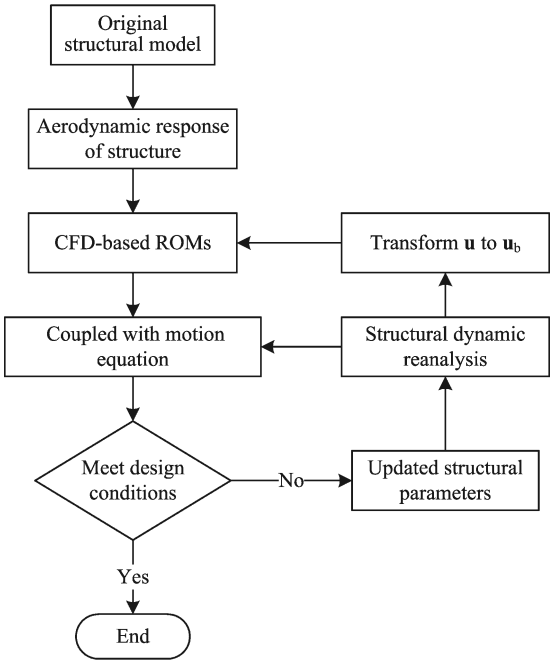

Fig. 2 Schematic of the aeroelastic ROM in the presence of global structural modifications.

The steps involved in this process are detailed in Algorithm 2.

Algorithm 2 Aeroelastic ROM for the modified structure	
1	For the original structure, generate the unsteady aerodynamics ROM;
2	Calculate coefficient matrix **Z** using the extended Kirsch combined method;
3	Perform transformation of coordinates to calculate the basic generalized displacements, $\mathbf{u}_b$;
4	Calculate the generalized aerodynamic force coefficients, $\mathbf{f}^{ext}$;
5	Couple fluid ROM, Eq. (32), with structural dynamics, Eq. (33) for the modified structure.

4. Numerical results and discussion

4.1 Validation of Aeroelastic ROM Solver

The first step is to establish the validity of the proposed aeroelastic ROM in predicting the flutter boundary for the AGARD 445.6 wing. The comparison is made with results obtained from the large-scale aeroelastic model, which employs the CFD solver rather than the unsteady aerodynamics ROM, and with experimental measurements [54]. The AGARD 445.6 wing model has a quarter-chord sweep angle of 45 deg, panel aspect ratio of 1.6525, and taper ratio of 0.6576. The symmetrical NACA65A004 airfoil section is used, governing the thickness distribution of the wing in the span-wise direction. The wing material has a density of 381.98 $\mathrm{Kg/m^3}$. The elastic moduli in the span-wise and chord-wise direction are 3.151 and 0.416 GPa, respectively, and the shear modulus is 0.4392 GPa. The Poisson's

ratio is 0.31 [55]. The structural model, shown in **Fig. 3**(a), consists of 231 nodes and 200 elements.

A multi-block structured mesh was employed for the flow predictions, consisting of 61 computational nodes around each airfoil section and 20 nodes along the wing semi-span, as shown in **Fig. 3**(b). The spatial convergence of the CFD mesh was analyzed in Zhou [23], where a good agreement of the results for both the medium and fine grids was documented. The total number of grid points on the medium grid, herein used, is 223,146 ($99\times49\times46$).

Fig. 4 shows the flutter boundary predictions from the large-scale aeroelastic model and the aeroelastic ROM. The ROM results are in good agreement with the reference numerical data for the entire range in Mach number (0.499 to 1.141). Physical effects, such as the transonic dip of the flutter speed, are correctly identified [56]. The accuracy of both methods was evaluated over the years in a number of aeroelastic studies [19, 23, 44].

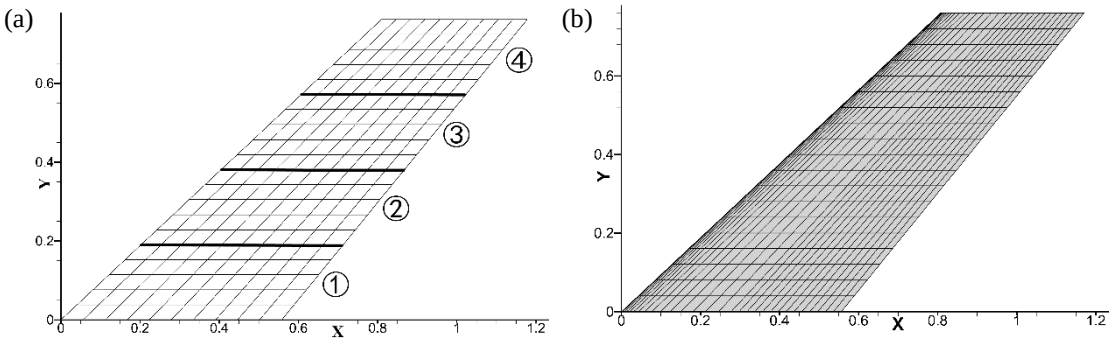

Fig. 3 AGARD 445.6 wing: (a) structural model, and (b) surface CFD mesh.

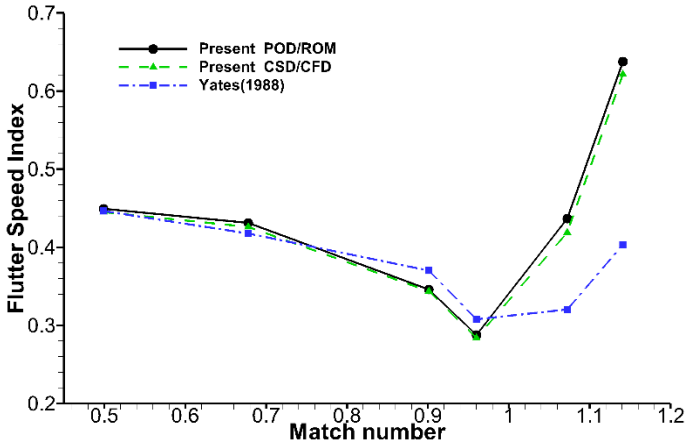

Fig. 4 AGARD 445.6 wing: flutter boundary; experimental data from Ref [54].

4.2 Validation of Structural Dynamic Reanalysis Method

For exemplification, the structural model of the AGARD 445.6 wing is divided into four span-wise sections, as shown in **Fig. 3**(a). Each section consists of 50 structural elements of identical material properties, but material properties at different sections may be different. To obtain global variations of

the mass and stiffness distribution, material properties are assumed to vary as

$$\text{Section 1,}\quad E_1 = (1+3\varepsilon)E_0\,, \qquad \rho_1 = (1+3\varepsilon)\rho_0$$

$$\text{Section 2,}\quad E_2 = (1+2\varepsilon)E_0\,, \qquad \rho_2 = (1+2\varepsilon)\rho_0$$

$$\text{Section 3,}\quad E_3 = (1+\varepsilon)E_0\,, \qquad \rho_3 = (1+\varepsilon)\rho_0$$

$$\text{Section 4,}\quad E_4 = E_0\,, \qquad \rho_4 = \rho_0$$

where E_0 and ρ_0 are the Young's modulus and density, respectively, of the baseline (original) structural model. It is worth observing that the choice above is used for demonstration purposes and shall not be taken here as a limiting case of the present method. On the contrary, material properties may be thought to vary independently on every single structural element, as commonly practiced in an aeroelastic tailoring study. To assess the accuracy of the ROM in analyzing the modal characteristics of the modified structural model, two criteria are introduced. The first criterion represents the error of the modal frequencies:

$$Error = \frac{f_A^i - f_E^i}{f_E^i} \tag{34}$$

where f_E^i denotes the exact modal frequencies, which are computed with a direct full modal analysis, and f_A^i denotes the approximate modal frequencies obtain by the Extended Kirsch combined method. The second criterion is the Modal Assurance Criterion (MAC), defined as:

$$\text{MAC}(\boldsymbol{\Phi}_A, \boldsymbol{\Phi}_E) = \frac{\left|\boldsymbol{\Phi}_E^T \boldsymbol{\Phi}_A\right|^2}{(\boldsymbol{\Phi}_A^T \boldsymbol{\Phi}_A)(\boldsymbol{\Phi}_E^T \boldsymbol{\Phi}_E)} \tag{35}$$

where $\boldsymbol{\Phi}_E$ represents the exact modeshapes (direct full modal analysis), and $\boldsymbol{\Phi}_A$ represents the approximate modeshapes (Extended Kirsch combined method). For a perfect match between the exact and approximate modeshape, the MAC is 1.

Three cases for the modified structure are considered: $\varepsilon = 1/12,\ 1/6,\ 1/3$. **Fig. 5** illustrates the modeshapes for the original (AGARD 445.6 wing) and modified wing models. For conciseness, only the case with the largest structural modifications ($\varepsilon = 1/3$) is reported. Modal information for the modified structure was obtained using the direct full modal method, which provides the exact reference data, and the approximate method based on the extended Kirsch combined approach. The first four modeshapes are identified to be the first bending, first torsional, second bending, and second torsional modes. Quantitatively, the errors between approximate and exact solutions are summarized in **Table 1** for the three values of the modification parameter, ε. For all cases, the error of the modal frequencies is well

below one percent. For the MAC, values near unity indicate a good to excellent agreement between the modeshapes of the approximate and exact solutions. The comparison conveys the good predictive capability of the Extended Kirsch combined method to provide approximate modeshapes and frequencies, which are accurate for fast engineering applications, without resorting to a direct full modal analysis for each modified structural case.

Table 1 Frequencies from direct and approximate structural reanalysis methods for the modified structural model of the AGARD 445.6 wing.

Parameter	Mode	Frequency [Hz]		Error [%]	MAC
		Exact	Approximate		
$\varepsilon = 1/12$	1	10.208	10.207	-0.005	1.0000
	2	41.228	41.232	0.010	0.9999
	3	50.756	50.792	0.071	0.9998
	4	95.962	96.034	0.076	0.9991
$\varepsilon = 1/6$	1	10.854	10.856	0.021	1.0000
	2	42.457	42.470	0.030	0.9998
	3	51.819	51.930	0.220	0.9993
	4	96.633	96.873	0.248	0.9970
$\varepsilon = 1/3$	1	11.933	11.943	0.082	0.9999
	2	44.354	44.398	0.101	0.9994
	3	53.591	53.894	0.565	0.9991
	4	97.712	98.412	0.716	0.9911

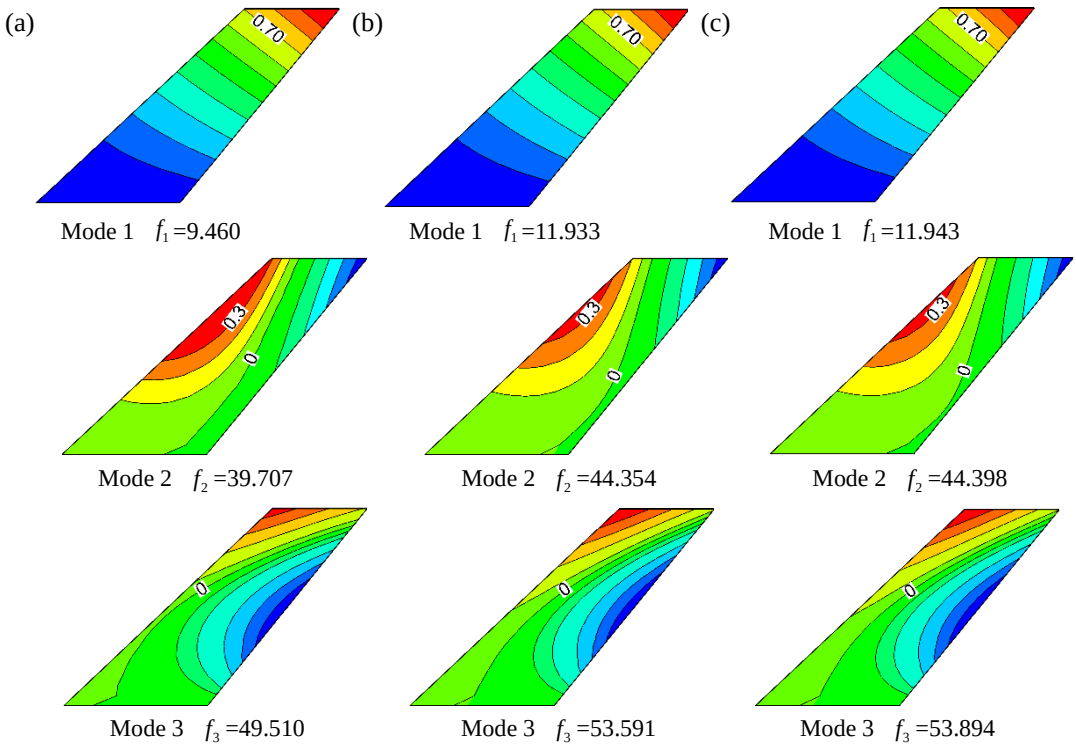

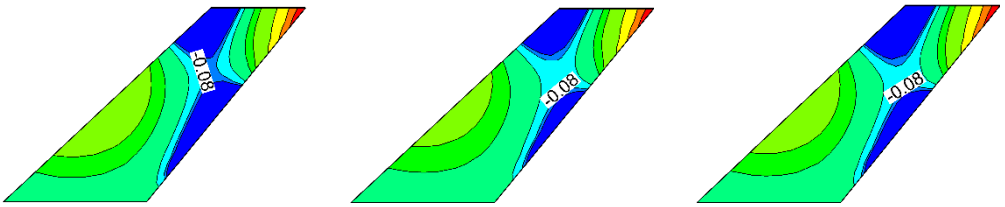

Mode 4 f_4 =95.134 Mode 4 f_4 =97.712 Mode 4 f_4 =98.412

Fig. 5 AGARD 445.6 wing: first four modeshapes. In (a), original structural model. In (b), exact solution (direct full modal method) and, in (c), approximate solution (extended Kirsch combined method) for the large structural modification case ($\varepsilon = 1/3$).

4.3 Aeroelastic Predictions in the Presence of Global Structural Modifications

The proposed approximate aeroelastic ROM valid for global structural modifications consists of two building blocks: the unsteady aerodynamics ROM and the structural reanalysis methods. Having validated these building blocks, we turn our attention to aeroelastic predictions in the presence of global structural modifications.

Fig. 6 reports the time history of the generalized aerodynamic forces (GAF) computed at $\mathrm{Ma} = 0.960$ and AOA=0 *deg* for two speeds ($V_\infty = 340$ m/s and $V_\infty = 375$ m/s). Two sets of data are compared. One set is representative of the large scale aeroelastic model, whereby the CFD solver is used for the aerodynamic predictions and the modal properties of the structure are re-computed at each structural modification. In the figures, data are labelled 'Exact Model' from here onwards. The second set of data is for the aeroelastic ROM, which employs a POD-based ROM for the aerodynamic predictions and the approximated reanalysis method is used to account for the influence of structural modifications. In the figures, these data are labelled 'Approximate ROM' from here onwards. A close inspection reveals that results from the direct and the proposed approximate ROM methods are in reasonable agreement for the case of the largest structural modification ($\varepsilon = 1/3$). A similar agreement was found for the smaller structural modifications, but results are not reported herein for brevity.

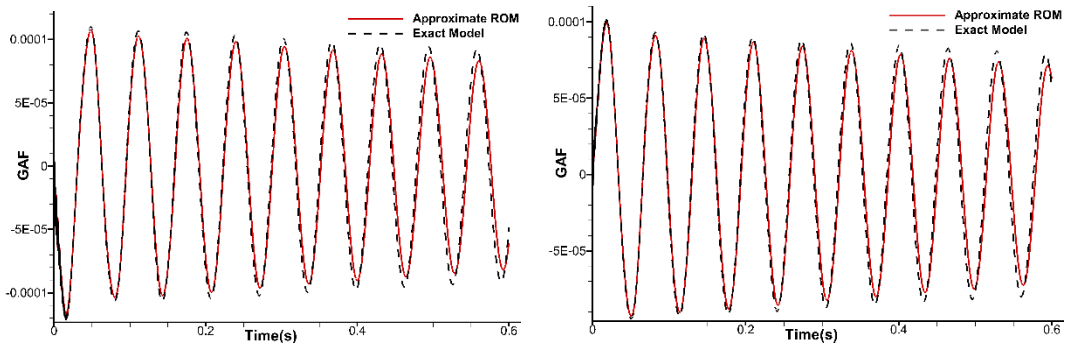

(a) GAF, first bending mode (b) GAF, first torsional mode

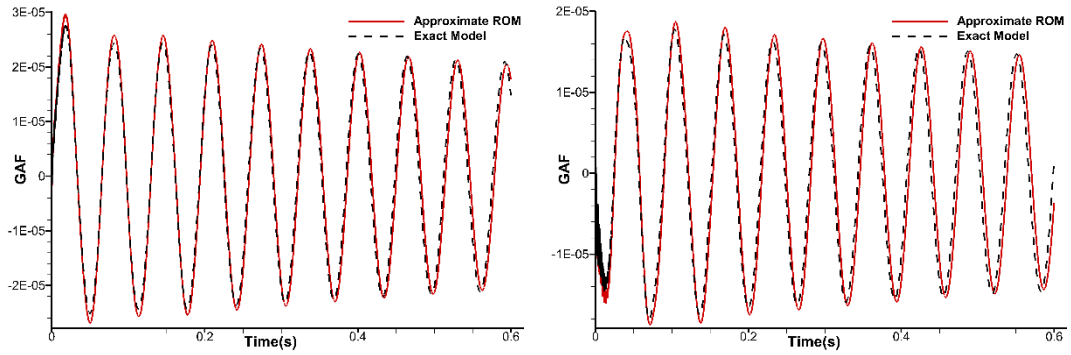

(c) GAF, second bending mode (d) GAF, second torsional mode

Fig. 6 Generalized aerodynamic forces for the largest structural modification ($\varepsilon = 1/3$) at M = 0.960, AOA = 0 *deg* .

To demonstrate further the predictive capability of the aeroelastic ROM, two typical aeroelastic responses (decaying and diverging) are compared in **Figs. 7** to **9**. Each figure corresponds to a different structural modification case, and the freestream speed (or equivalently the dynamic pressure) was chosen to observe a stable and unstable aeroelastic response. It was found that the aeroelastic ROM is capable to predict the loss of the system stability for all structural modification cases. The ROM predictions follow closely those of the large-scale aeroelastic model.

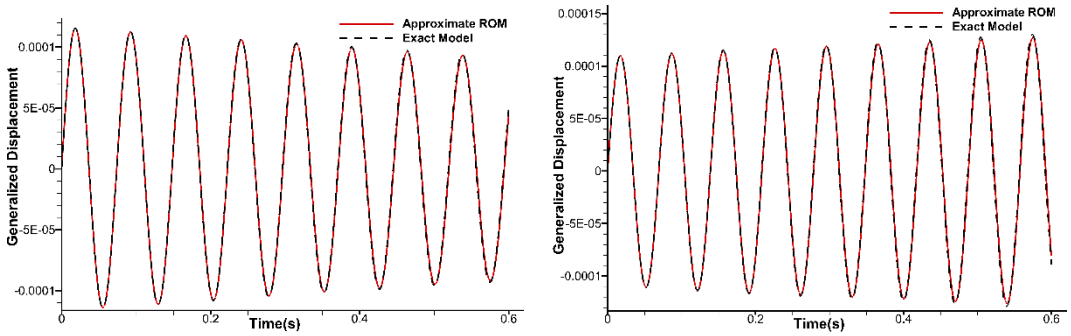

(a) Generalized displacements, first bending mode (left: $V_\infty = 290$ m/s, right: $V_\infty = 320$ m/s)

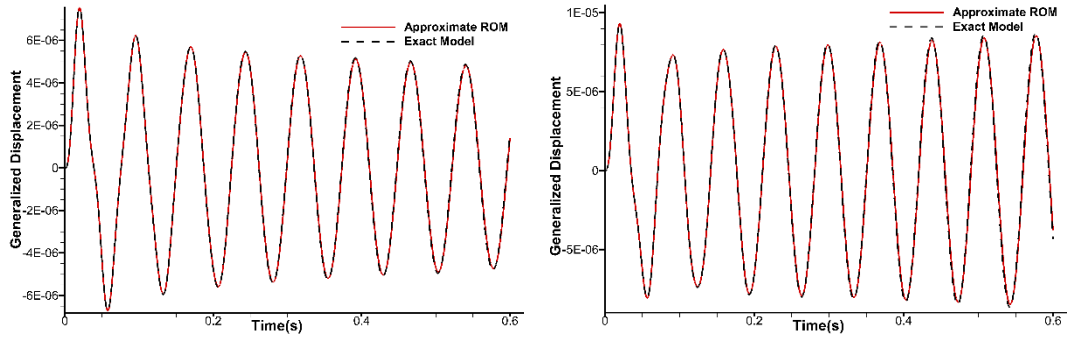

(b) Generalized displacements, first torsional mode (left: $V_\infty = 290$ m/s, right: $V_\infty = 320$ m/s)

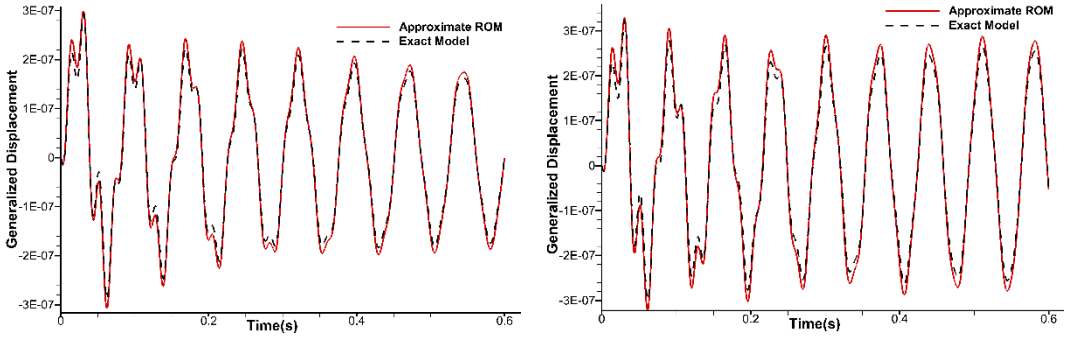

(c) Generalized displacements, second bending mode (left: $V_\infty = 290$ m/s, right: $V_\infty = 320$ m/s)

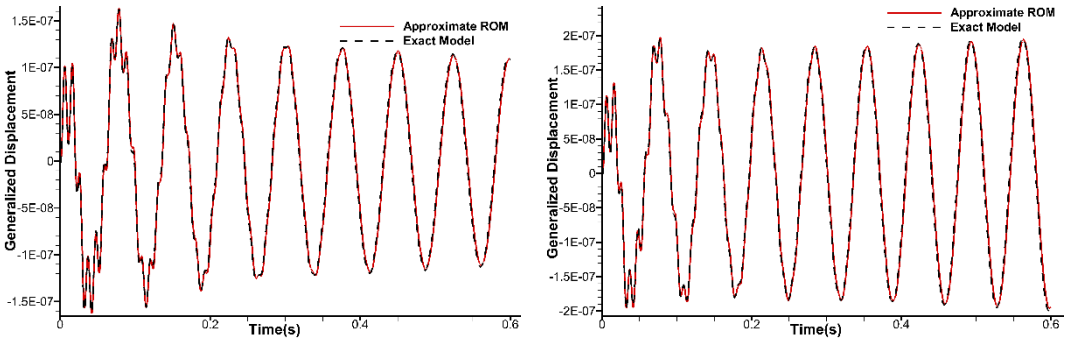

(d) Generalized displacements, second torsional mode (left: $V_\infty = 290$ m/s, right: $V_\infty = 320$ m/s)

Fig. 7 Generalized displacements for the smallest structural modification ($\varepsilon = 1/12$) at two freestream speeds; flow conditions: M = 0.960, AOA = 0 *deg* .

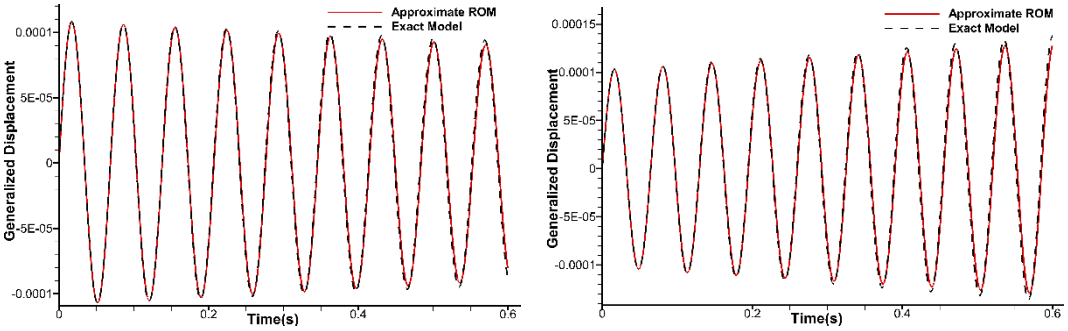

(a) Generalized displacements, first bending mode (left: $V_\infty = 315$ m/s, right: $V_\infty = 345$ m/s)

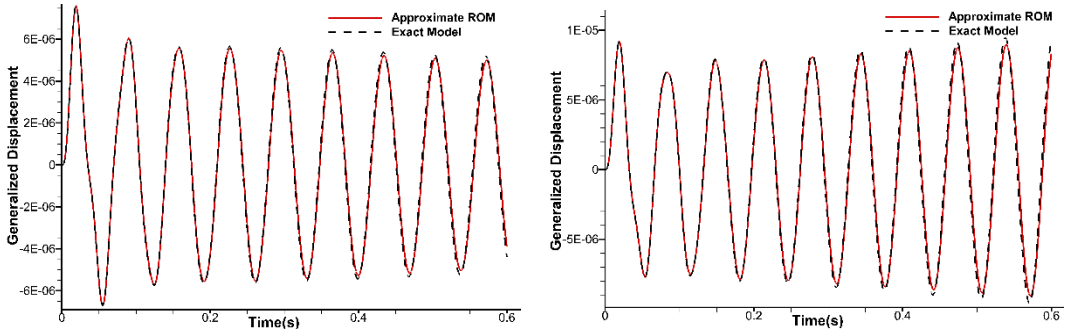

(b) Generalized displacements, first torsional mode (left: $V_\infty = 315$ m/s, right: $V_\infty = 345$ m/s)

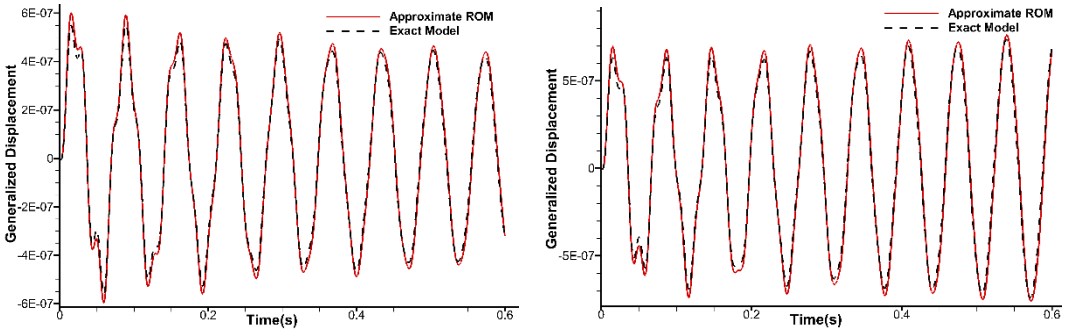

(c) Generalized displacements, second bending mode (left: $V_\infty = 315$ m/s, right: $V_\infty = 345$ m/s)

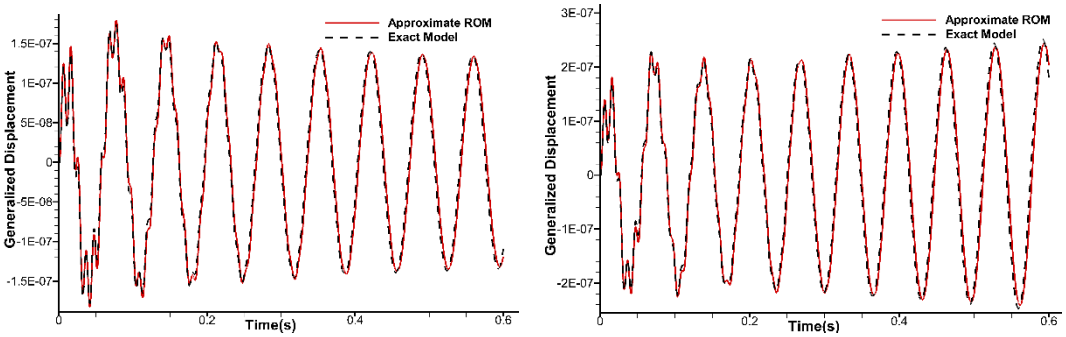

(d) Generalized displacements, second torsional mode (left: $V_\infty = 315$ m/s, right: $V_\infty = 345$ m/s)

Fig. 8 Generalized displacements for the medium structural modification ($\varepsilon = 1/6$) at two freestream speeds; flow conditions: M = 0.960, AOA = 0 *deg* .

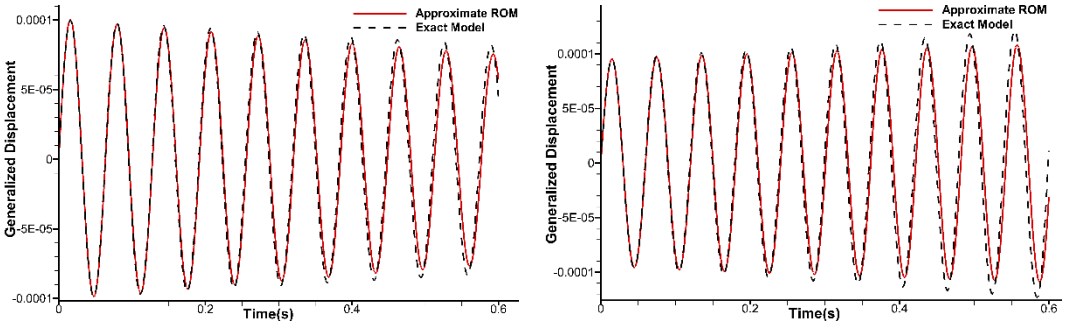

(a) Generalized displacements, first bending mode (left: $V_\infty = 340$ m/s, right: $V_\infty = 375$ m/s)

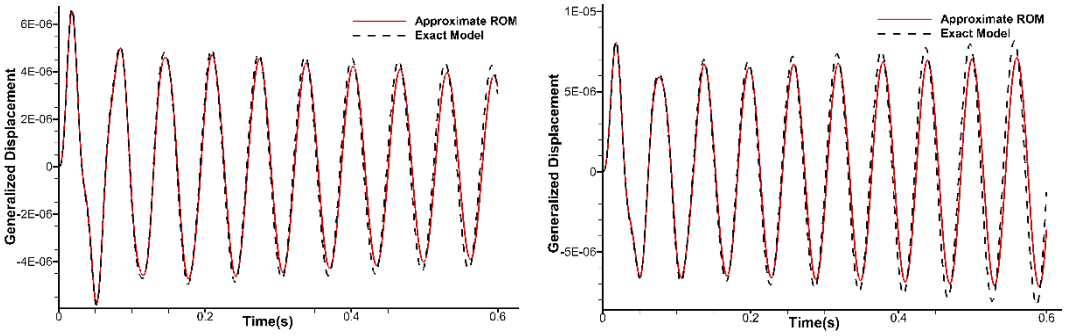

(b) Generalized displacements, first torsional mode (left: $V_\infty = 340$ m/s, right: $V_\infty = 375$ m/s)

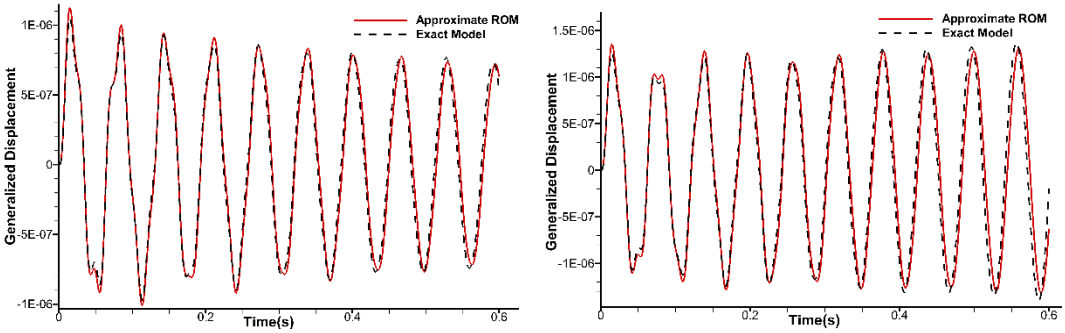

(c) Generalized displacements, second bending mode (left: $V_\infty = 340$ m/s, right: $V_\infty = 375$ m/s)

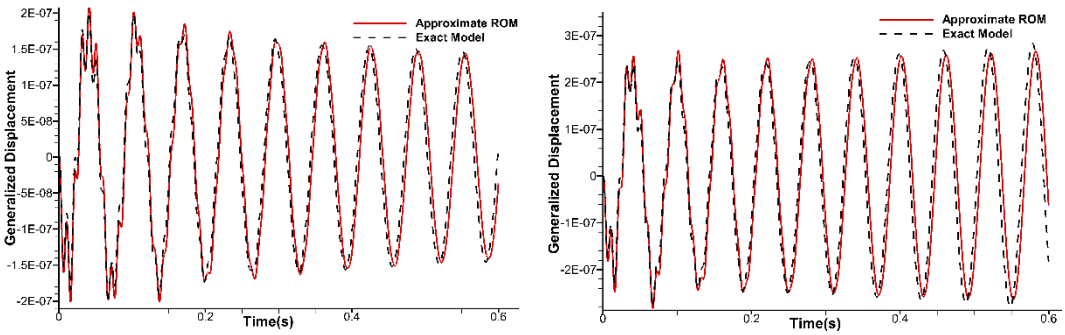

(d) Generalized displacements, second torsional mode (left: $V_\infty = 340$ m/s, right: $V_\infty = 375$ m/s)

Fig. 9 Generalized displacements for the largest structural modification ($\varepsilon = 1/3$) at two freestream speeds; flow conditions: M = 0.960, AOA = 0 *deg* .

Finally, we employ the aeroelastic ROM to investigate the impact that the structural modification has on the flutter speed. The flutter problem is solved through an eigenvalue analysis, tracking the freestream speed at which the eigenvalue with the largest real part crosses the imaginary axis. Results are illustrated in **Fig. 10** for the three different levels of structural modifications ($\varepsilon = 1/12,\ 1/6,\ 1/3$). The overall behavior is captured reasonably well, also away from the flutter occurrence, by the aeroelastic ROM. It is not unexpected that the predictions degrade for increasing structural modifications.

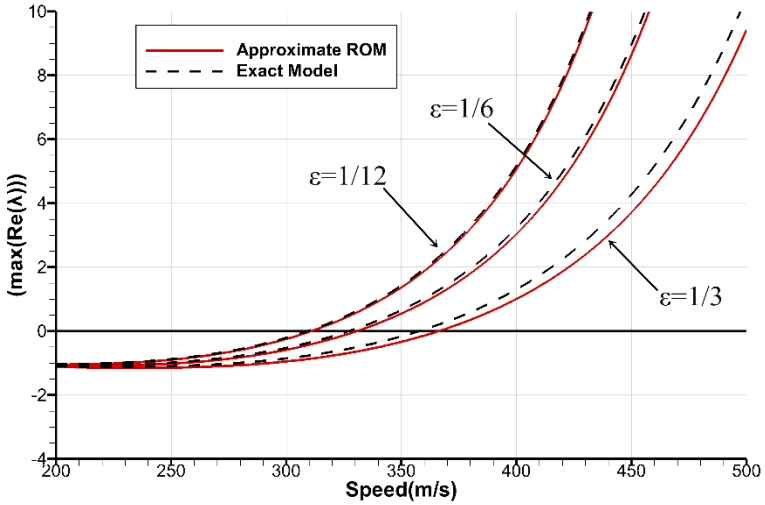

Fig. 10 Dependence of the system eigenvalue with the largest real part on freestream speed (M = 0.960, AOA = 0 *deg*).

A quantification of the error introduced to predict the flutter speed using the aeroelastic ROM is presented in **Table 2**. Reference data are taken from the large-scale aeroelastic model, as already pointed out. Although the discrepancy between the two methods increase for increasing level of the structural modifications, it is worth observing that the maximum difference is limited to about 2% for the largest modification ($\varepsilon = 1/3$) of the structure.

Table 2 Flutter speed obtained by direct and approximate method at Ma=0.960.

Parameter	Flutter speed (m/s)		
	Direct method	Approximate method	Error (%)
$\varepsilon = 1/12$	309.2	310.8	0.518
$\varepsilon = 1/6$	327.2	330.7	1.070
$\varepsilon = 1/3$	357.7	365.6	2.210

4.4 Computational Costs

A final consideration is for the computational cost associated with the analyses presented in this work. All analyses were performed on a Windows 7 system PC with Intel® Core(TM) i7-2600 CPU (3.40 GHz, 8 cores, but only one core used) and 16 GB RAM. The timing in **Table 3** is given for this type of machine, but here it is of great interest to analyze the speed-up of the approximate aeroelastic ROM in comparison to the aeroelastic ROM that solves the structural eigenvalue problem and a new set of POD modes at each structural design iteration. For the direct method, a set of POD modes is generated for each structural modification, requiring about 16*h* per configuration. The response in the time domain is inexpensive. For the three structural modifications, the aeroelastic model employing the direct eigenvalue method required about 48*h*. In contract to this, the set of POD modes is calculated only once for the approximate aeroelastic ROM. Subsequent steps, as detailed in Algorithm 2, have negligible computational costs. For the three structural modifications, the approximate aeroelastic model required about 16*h*.

The computational efficiency of the approximate aeroelastic ROM derives from calculating only once the set of POD modes. With the ability to treat efficiently modifications to the structural model, the computational advantage of the approximate aeroelastic ROM becomes more significant the more changes to the structure are considered. Within the work presented in this manuscript, the speed-up of the approximate aeroelastic ROM compared to the direct model is about three, which is proportional to the number of structural modifications. However, within an industrial design process, it is reasonable to

consider about 1,000 structural modifications and 20 values of the freestream dynamic pressure to assess the aeroelastic stability. With information reported in **Table 3**, the direct method would require over 16 thousand CPU hours (this consists of $16h \times 1000$ and $1.75s \times 20 \times 1000$, totaling $16{,}009.72h$), whereas the approximate aeroelastic ROM just over 26 CPU hours ($16h \times 1$ and $1.79s \times 20 \times 1000$, totaling $25.94h$). The expected speed-up is proportional with the number of structural modifications, making the proposed approximate aeroelastic ROM adequate for optimization and uncertainty studies.

Table 3 Computational costs of direct and approximate aeroelastic ROMs.

Method	Process	CPU time
Direct	Generate set of POD modes, per case	16*h*
	Calculate time response, per values of dynamic pressure	1.75s
	Three structural modifications	48*h* 5.25*s*
	Prototype problem with 1,000 structural modifications and 20 values of dynamic pressure	16,097.22*h*
Approximate	Generate set of POD modes for original structure	16*h*
	Compute **Z** with Extended Kirsch combined method	0.76*s*
	Calculate time response, per values of dynamic pressure	1.79*s*
	Three structural modifications	16*h* 18.39*s*
	Prototype problem with 1,000 structural modifications and 20 values of dynamic pressure	26.16*h*

5. Conclusions

The work summarized in this manuscript discusses an efficient aeroelastic reduced order model in the presence of global modifications of the structure. Structural properties are subject to large variations from the initial configuration, in a similar manner to the iterative changes explored within the aircraft design process. The computational challenges that arise when dealing with this problem are two-folded. The first challenge concerns with the calculation of the time domain aeroelastic response using computational fluid dynamics. This task is computationally intensive for the stringent stability limits imposed by the fluid system, even assuming the most favorable situation where the structure is frozen. The second aspect arises when the structure undergoes iteratively large changes from the initial design, adding extra costs that easily make the total computing cost prohibitive for routine applications.

The manuscript proposes a method to overcome the problems highlighted in the previous paragraph. The method builds on various elements, which are described, validated, and demonstrated throughout the manuscript. Two algorithms are given, and it is the hope these will support the application of the methods to other engineering fields. The method consists of: a) a proper orthogonal decomposition of

the linearized Navier-Stokes equations, calculated around an aeroelastic equilibrium point, in turn, dependent upon the structural model; the decomposition allows reducing the size of the fluid system; b) a structural dynamic reanalysis method that allows calculating the frequencies and modeshapes of the modified structure without solving the corresponding eigenvalue problem at each change of the structural model; the method builds on the extended Kirsch combined method; and c) a mechanism to exchange information between fluid and structural solvers without need for calculating at each iteration of the structural design an eigenvalue problem of the modified structure, or a new set of modes for the fluid decomposition.

Results were obtained for the AGARD 445.6 wing. Material properties of the structure were varied up to 100% of their nominal values. After a validation of each constitutive element, the proposed aeroelastic reduced order model was tested for predictions of the time domain generalized aerodynamic loads and displacements, and of the flutter speed in the presence of global modifications of the structure. The comparison was made with a standard aeroelastic reduced order model which solves for the structural eigenvalue problem and for a new set of modes for the fluid decomposition at each structural design change. For the prototype problem, the proposed method was found to retain high efficiency and good accuracy in comparison with the standard model. The computational efficiency of the proposed method, which generates only once the set of modes for the fluid system, grows linearly with the number of structural changes. It is therefore ideally placed for applications in optimization and uncertainty analysis.

A final observation is for the reduced order model of the fluid system. The proposed method is not restricted to a specific type of aerodynamics, such as proper orthogonal decomposition as in this case. It is, on the contrary, a general-purpose approach that may be coupled with alternative reduced order models of unsteady aerodynamics.

Acknowledgments

This work was partially supported by the National Natural Science Foundation of China (No. 11672225, 11511130053 and 11272005), the National Program on Key Research Projects (No. MJ-2015-F-010), the Shannxi Province Natural Science Foundation (No. 2016JM1007), and the founds for the Central Universities (2014XJJ0126).

References

[1] G.P. Guruswamy, Unsteady aerodynamic and aeroelastic calculations for wings using Euler equations, AIAA journal, 28 (1990) 461-469.

[2] J. Sahu, F. Fresconi, K. Heavey, Unsteady Aerodynamic Simulations of a Finned Projectile at a Supersonic Speed with Jet Interaction, 32nd AIAA Applied Aerodynamics Conference, 2014, pp. 3024.

[3] D.M. Schuster, D.D. Liu, L.J. Huttsell, Computational aeroelasticity: success, progress, challenge, Journal of Aircraft, 40 (2003) 843-856.

[4] R. Yurkovich, Status of unsteady aerodynamic prediction for flutter of high-performance aircraft, Journal of Aircraft, 40 (2003) 832-842.

[5] D.E. Raveh, Reduced-Order Models for Nonlinear Unsteady Aerodynamics, Aiaa Journal, 39 (2011) 1417-1429.

[6] W.A. Silva, R.E. Bartels, Development of reduced-order models for aeroelastic analysis and flutter prediction using the CFL3Dv6.0 code, Journal of Fluids & Structures, 19 (2004) 729-745.

[7] Z. Yang, R. Huang, Y. Zhao, H. Hu, Design of an Active Disturbance Rejection Control for Transonic Flutter Suppression, Journal of Guidance Control & Dynamics, DOI (2017) 1-12.

[8] E.H. Dowell, J.P. Thomas, K.C. Hall, Transonic limit cycle oscillation analysis using reduced order aerodynamic models, Journal of Fluids and Structures, 19 (2004) 17-27.

[9] D.J. Lucia, P.S. Beran, P.I. King, Reduced-order modeling of an elastic panel in transonic flow, Journal of Aircraft, 40 (2003) 338-347.

[10] D.E. Raveh, Gust-response analysis of free elastic aircraft in the transonic flight regime, Journal of Aircraft, 48 (2011) 1204-1211.

[11] P.G. A. Cizmas, A. Palacios, Proper orthogonal decomposition of turbine rotor-stator interaction, Journal of propulsion and power, 19 (2003) 268-281.

[12] S.T. Clark, R.E. Kielb, K.C. Hall, Developing a Reduced-Order Model to Understand Non-Synchronous Vibration (NSV) in Turbomachinery, ASME Turbo Expo 2012: Turbine Technical Conference and Exposition, 2012, pp. 1373-1382.

[13] S. Mariappan, A.D. Gardner, R. Kai, M. Raffel, Analysis of Dynamic Stall Using Dynamic Mode Decomposition Technique, Aiaa Journal, 52 (2014) 2427-2439.

[14] B. Stanford, P. Beran, Cost reduction techniques for the structural design of nonlinear flapping wings, 50th AIAA/ASME/ASCE/AHS/ASC Structures, Structural Dynamics, and Materials Conference 17th AIAA/ASME/AHS Adaptive Structures Conference 11th AIAA No, 2009, pp. 2414.

[15] L. Demasi, A. Palacios, A reduced order nonlinear aeroelastic analysis of joined wings based on the proper orthogonal decomposition, 51st AIAA/ASME/ASCE/AHS/ASC Structures, Structural Dynamics, and Materials Conference 18th AIAA/ASME/AHS Adaptive Structures Conference 12th, 2010, pp. 2722.

[16] H. Hesse, R. Palacios, Reduced-order aeroelastic models for dynamics of maneuvering flexible aircraft, AIAA journal, 52 (2014) 1717-1732.

[17] T. Lieu, C. Farhat, M. Lesoinne, Reduced-order fluid/structure modeling of a complete aircraft configuration, Computer methods in applied mechanics and engineering, 195 (2006) 5730-5742.

[18] D. Amsallem, C. Farhat, T. Lieu, Aeroelastic analysis of F-16 and F-18/A configurations using adapted CFD-based reduced-order models, 48th AIAA/ASME/ASCE/AHS/ASC Structures, Structural Dynamics, and Materials Conference, 2007, pp. 2364.

[19] Q. Zhou, G. Chen, Y. Li, a Reduced Order Model Based on Block Arnoldi Method for Aeroelastic System, International Journal of Applied Mechanics, 6 (2014) 1450069.

[20] G. Chen, X. Wang, Y. Li, REDUCED-ORDER-MODEL-BASED PLACEMENT OPTIMIZATION OF MULTIPLE CONTROL SURFACES FOR ACTIVE AEROELASTIC CONTROL, International Journal of

Computational Methods, 11 (2014) 1350081.
[21] G. Chen, J. Sun, W. Mao, Y. Li, Limit Cycle Oscillation Control for Transonic Aeroelastic Systems Based on Support Vector Machine Reduced Order Model, Transactions of the Japan Society for Aeronautical and Space Sciences, 56 (2013) 8-14.
[22] Q. Zhou, C. Gang, L. Yueming, D.R. Andrea, Aeroelastic Moving Gust Responses and Alleviation based on CFD, AIAA Modeling and Simulation Technologies Conference, 2016, pp. 3837.
[23] Q. Zhou, D.-f. Li, A. Da Ronch, G. Chen, Y.-m. Li, Computational fluid dynamics-based transonic flutter suppression with control delay, Journal of Fluids and Structures, 66 (2016) 183-206.
[24] B.I. Epureanu, E.H. Dowell, K.C. Hall, Mach number influence on reduced-order models of inviscid potential flows in turbomachinery, Journal of fluids engineering, 124 (2002) 977-987.
[25] T. Lieu, C. Farhat, Adaptation of POD-based aeroelastic ROMs for varying mach number and angle of attack: application to a complete F-16 configuration, AIAA paper, 7666 (2005) 2005.
[26] T. Lieu, C. Farhat, Adaptation of aeroelastic reduced-order models and application to an F-16 configuration, AIAA journal, 45 (2007) 1244-1257.
[27] T. Lieu, M. Lesoinne, Parameter adaptation of reduced order models for three-dimensional flutter analysis, AIAA Paper, 888 (2004) 2004.
[28] G. Chen, Y. Li, G. Yan, A nonlinear POD reduced order model for limit cycle oscillation prediction, Science China Physics, Mechanics and Astronomy, 53 (2010) 1325-1332.
[29] G. Chen, Y. Zuo, J. Sun, Y. Li, Support-vector-machine-based reduced-order model for limit cycle oscillation prediction of nonlinear aeroelastic system, Mathematical problems in engineering, 2012 (2012).
[30] C. Gang, S. Jian, L. Yueming, Active flutter suppression control law design method based on balanced proper orthogonal decomposition reduced order model, Nonlinear Dynamics, 70 (2012) 1-12.
[31] M. Winter, C. Breitsamter, Neurofuzzy-Model-Based Unsteady Aerodynamic Computations Across Varying Freestream Conditions, Aiaa Journal, 54 (2016) 1-16.
[32] R. Hayes, W. Yao, S.P. Marques, The Influence of Structural Variability on Limit Cycle Oscillation Behaviour, Aiaa/issmo Multidisciplinary Analysis and Optimization Conference, 2014, pp. 63.
[33] C. Fenwick, D. Jones, A. Gaitonde, Consideration of ROM Interpolation for Aeroelastic Design using Structural Modification, 18th AIAA Computational Fluid Dynamics Conference, Miami, FL, 2007.
[34] R. Voss, L. Tichy, R. Thormann, A ROM based flutter prediction process and its validation with a new reference model, IFASD 2011 - International Forum on Aeroelasticity and Structural Dynamics, 2011.
[35] W. Zhang, K. Chen, Z. Ye, Unsteady aerodynamic reduced-order modeling of an aeroelastic wing using arbitrary mode shapes, Journal of Fluids & Structures, 58 (2015) 254-270.
[36] M. Winter, F.M. Heckmeier, C. Breitsamter, CFD-based aeroelastic reduced-order modeling robust to structural parameter variations, Aerospace Science & Technology, 67 (2017) 13-30.
[37] P. Gasbarri, L.D. Chiwiacowsky, H.F.D.C. Velho, A hybrid multilevel approach for aeroelastic optimization of composite wing-box, Structural & Multidisciplinary Optimization, 39 (2010) 607-624.
[38] P.D. Ciampa, B. Nagel, M. Van Tooren, Global local structural optimization of transportation aircraft wings, 51st AIAA/ASME/ASCE/AHS/ASC Structures, Structural Dynamics, and Materials Conference, Orlando, USA, April 2010, 2010.
[39] B. Van Leer, Towards the ultimate conservative difference scheme. V. A second-order sequel to Godunov's method, Journal of computational Physics, 32 (1979) 101-136.
[40] T. PULLIAM, Time accuracy and the use of implicit methods, 11th Computational Fluid Dynamics Conference, 1993, pp. 3360.
[41] R. Chen, Z. Wang, Fast, block lower-upper symmetric Gauss-Seidel scheme for arbitrary grids, AIAA journal,

38 (2000) 2238-2245.
[42] R.L. Harder, R.N. Desmarais, Interpolation using surface splines, Journal of aircraft, 9 (1972) 189-191.
[43] H. Tsai, A. F. Wong, J. Cai, Y. Zhu, F. Liu, Unsteady flow calculations with a parallel multiblock moving mesh algorithm, AIAA journal, 39 (2001) 1021-1029.
[44] G. Chen, J. Sun, Y.-M. Li, Adaptive reduced-order-model-based control-law design for active flutter suppression, Journal of Aircraft, 49 (2012) 973-980.
[45] K.C. Hall, J.P. Thomas, E.H. Dowell, Proper orthogonal decomposition technique for transonic unsteady aerodynamic flows, AIAA journal, 38 (2000) 1853-1862.
[46] T. Lieu, C. Farhat, M. Lesoinne, POD-based aeroelastic analysis of a complete F-16 configuration: ROM adaptation and demonstration, 46th AIAA/ASME/ASCE/AHS/ASC Structures, Structural Dynamics and Materials Conference, 2005, pp. 2295.
[47] Q. Song, P. Chen, S. Sun, An exact reanalysis algorithm for local non-topological high-rank structural modifications in finite element analysis, Computers & Structures, 143 (2014) 60–72.
[48] M.A. Akgün, J.H. Garcelon, R.T. Haftka, Fast exact linear and non‐linear structural reanalysis and the Sherman–Morrison–Woodbury formulas, International Journal for Numerical Methods in Engineering, 50 (2001) 1587-1606.
[49] J.-G. Beliveau, S. Cogan, G. Lallement, F. Ayer, Iterative least-squares calculation for modal eigenvector sensitivity, AIAA journal, 34 (1996) 385-391.
[50] S.H. Chen, X.W. Yang, Extended Kirsch combined method for eigenvalue reanalysis, AIAA journal, 38 (2000) 927-930.
[51] U. Kirsch, M. Bogomolni, I. Sheinman, Efficient Dynamic Reanalysis of Structures, Journal of Structural Engineering, 133 (2007) 440-448.
[52] S. Chen, X. Yang, H. Lian, Comparison of several eigenvalue reanalysis methods for modified structures, Structural and Multidisciplinary Optimization, 20 (2000) 253-259.
[53] S.H. Chen, D.T. Song, A.J. Ma, Eigensolution reanalysis of modified structures using perturbations and Rayleigh quotients, Communications in numerical methods in engineering, 10 (1994) 111-119.
[54] E.C. Yates, AGARD standard aeroelastic configuration for dynamic response, candidate configuration I, Wing, 445 (1987) 103-129.
[55] J. Zhong, Z. Xu, Coupled fluid structure analysis for wing 445.6 flutter using a fast dynamic mesh technology, International Journal of Computational Fluid Dynamics, 30 (2016) 531-542.
[56] W.A. Silva, P. Chwalowski, B.P. Iii, Evaluation of linear, inviscid, viscous, and reduced-order modelling aeroelastic solutions of the AGARD 445.6 wing using root locus analysis, International Journal of Computational Fluid Dynamics, 28 (2014) 122-139.